Tu P1 03

Velocity Building by Reflection Waveform Inversion without Cycle-skipping

Q. Guo* (KAUST), T. Alkhalifah (KAUST), Z. Wu (KAUST)

Summary

Reflection waveform inversion (RWI) provides estimation of low wavenumber model components using reflections generated from a migration/demigration process. The resulting model tends to be a good initial model for FWI. In fact, the optimization images to combine the migration velocity analysis (MVA) objectives (given here by RWI) and the FWI ones. However, RWI may still encounter cycle-skipping at far offsets if the velocity model is highly inaccurate. Similar to MVA, RWI is devoted to focusing reflection data to its true image positions, yet because of the cycle skipping potential we tend to initially use only near offsets. To make the inversion procedure more robust, we introduce the extended image into our RWI. Extending the model perturbations (or image) allows us to better fit the data at larger offsets even with an inaccurate velocity. Thus, we implement a nested approach to optimize the velocity and extended image simultaneously using the objective function of RWI. We slowly reduce the extension, as the image becomes focused, to allow wavepath updates from far offsets to near as a natural progression from long wavelength updates to shorter ones. Applications on synthetic data demonstrate the effectiveness of our method without much additional cost to RWI.

Introduction

Full waveform inversion (FWI) was first introduced to the seismic exploration community by Tarantola (1984), which is designed to provide a high resolution model of subsurface. However, in practice, FWI requires a kinematically correct initial model, otherwise it may fall into a local minimum solution. It means we need an approach, like migration velocity analysis (MVA) (Symes and Kern, 1994), to obtain the low wavenumber components of the model. Still a gap exists between the wavenumbers estimated by MVA and FWI (Claerbout, 1985). Actually, Mora (1989) stated that FWI is a process made up of tomography and imaging, and thus, building an optimal combination of MVA and FWI might be a natural one. Xu et al. (2012), following Plessix et al. (1995), introduced a feasible and cheaper approach to estimate the low wavenumber model components by using the reflections generated from the migration/demigration process instead of requiring a high wavenumber model to produce such reflections. The residuals between the original data and the demigrated one can be used to update the the velocity model along wavepaths. We refer to this approach as reflection waveform inversion (RWI), which has the ability to fill the gap between MVA and FWI (Alkhalifah and Wu, 2016).

Both RWI and MVA based on DSO aim at retrieving the low wavenumber components of the model by updating along reflection wavepaths. The objective function of MVA, even starting from a poor initial model, is still able to converge to a smooth solution. However, the limited aperture imposes some bias to the MVA result, which is not accurate enough for FWI in many cases. On the other hand, RWI produces relatively higher wavenumber wavepath updates as the matching criteria at the reference zero offset (and near offset) is weighted equally with the far offset, a feature not provided in DSO. However, RWI can include undesirable high wavenumber components (Wu and Alkhalifah, 2015) in real cases.

In this abstract, we redefine the extended imaging/modeling process and show the gradient with respect to velocity model using our previously proposed RWI objective function. In the inversion, we merge features of MVA by gradually reducing the volume of the extended image space, which at the end transitions to regular RWI. We test our method on a simple model to analyze its behavior, as well as the Marmousi example without low frequency data and compare those results with regular FWI.

Theory

Similar to the definition of subsurface offset extended Born modeling (Hou and Symes, 2015), which is derived from the concept of survey-sinking of the sources and receivers (Claerbout, 1985), we define our extended modeling as

$$\mathbf{F}\tilde{u}(s,\mathbf{x},t) = \int_h u(s,\mathbf{x}-\mathbf{h},t) \times I(\mathbf{x}-\mathbf{h},\mathbf{h}), \tag{1}$$

where $I(\mathbf{x},\mathbf{h})$ is our extended image, $\mathbf{h}$ only contains the horizontal component of the extension, $\tilde{u}(s,\mathbf{x},t)$ is the modeled acoustic wavefield for source, s ,and $\mathbf{F}$ is the wave equation operator, expressed here as

$$\mathbf{F} = \left(\frac{1}{c^2}\frac{\partial}{\partial t^2} - \nabla^2\right) \quad \& \quad \mathbf{F}u(s,\mathbf{x},t) = f. \tag{2}$$

The objective of this Born operator for us is to model a reflection waveform that fits the shape of the recorded one. With the adjoint-state method (Plessix, 2006), we can derive the adjoint operation with respect to the extended Born modeling, which is expressed as

$$\Delta I(\mathbf{x},\mathbf{h}) = \sum_s \int_t u(s,\mathbf{x},t) \times \tilde{\mu}(s,\mathbf{x}+\mathbf{h},t), \tag{3}$$

where $\tilde{\mu}(s,\mathbf{x},t)$ is the adjoint wavefield, which is calculated as

$$\mathbf{F}^*\tilde{\mu}(s,\mathbf{x},T-t) = \sum_r \left(\mathbf{A}[u+\tilde{u}]-d\right)(s,\mathbf{x}_r,T-t), \tag{4}$$

where **A** constrains the wavefield to the receiver positions and the right-hand side of equation is the data misfit. Given the correct velocity model, least-squares migration can map the recorded data to its true image position (Symes and Kern, 1994), with energy focusing on the zero subsurface offset. However, if the model is not kinematically correct, the migrated energy will be distributed to non-zero subsurface offsets. The added non-physical axis enables the demigration to produce reflections with better accuracy in both amplitude and phase.

Using the objective function, $E = \frac{1}{2}\sum_{s,r}\int dt|\mathbf{A}[u(s,\mathbf{x},t)+\tilde{u}(s,\mathbf{x},t)]-d_0|^2$ presented recently (Wu and Alkhalifah, 2015; Guo and Alkhalifah, 2016), we derive the gradient with respect to model parameter c, as follows

$$\frac{\partial E}{\partial c(\mathbf{x})} = -\sum_s \frac{1}{c}\int dt\left[\nabla^2\tilde{u}(s,\mathbf{x},t)\tilde{\mu}(s,\mathbf{x},t)+\nabla^2 u(s,\mathbf{x},t)\nu(s,\mathbf{x},t)+\nabla^2 u(s,\mathbf{x},t)\tilde{\mu}(s,\mathbf{x},t)\right], \quad (5)$$

where ν can be calculated using

$$\mathbf{F}^*\nu(s,\mathbf{x},T-t) = \int d\mathbf{h}\, I(\mathbf{x},\mathbf{h})\times\tilde{\mu}(s,\mathbf{x}+\mathbf{h},T-t), \quad (6)$$

which is the adjoint wavefield produced by perturbing $\tilde{\mu}$ at the estimated extended image.

As we can see in equation 5, the gradient with respect to the model parameter has a similar form as our previous one, in which the first term $\nabla^2\tilde{u}(s,\mathbf{x},t)\tilde{\mu}(s,\mathbf{x},t)$ and second term $\nabla^2 u(s,\mathbf{x},t)\nu(s,\mathbf{x},t)$ are the updates along reflection wavepath, which are our RWI terms; the third term $\nabla^2 u(s,\mathbf{x},t)\tilde{\mu}(s,\mathbf{x},t)$ is the familiar FWI term. The first two terms are expected to provide low wavenumber updates. Our estimation of velocity differs from the conventional RWI in two aspects: one is the computation of model perturbations, which is in the extended domain; another is in producing the perturbed field (and its adjoint). Since it is a linear operator, the extended space only results in some additional computational cost in the correlation operation, with no extension in memory requirement.

New Features of Extended RWI

Though RWI is an alternative approach to MVA, it still suffers from the cycle-skipping if we start from a reasonably poor initial model. The classic RWI splits the model into background, controlling the kinematic features, and perturbations, which mainly involves the energy at zero offset. The main difference between our extended RWI and the classic one is in including the extended image/Born model, which makes the objective function more convex. Thus, our new proposed RWI has a good opportunity to avoid local minima regardless of the starting velocity with the possibility of providing RWI resolution updates as we reduce the offset extension. Thus, our approach starts with allowing for a relatively large span of subsurface offsets **h** (not all), which is capable of capturing most of the energy imaged from the data short of the furthest offsets. Thus, the residuals at the far offsets are used in the RWI process to update the velocity model with the longest wavelengths. Specifically, we use the RWI terms of equation 5 to update the velocity model. Once we get a converged solution, we gradually reduce the extension volume, which will force us to fit the data with less subsurface offsets until the extension is zero. In this case, our approach will ultimately reduce to a conventional RWI, which utilizes the data residuals at full offsets without cycle-skipping, thus, the additional cost only exists at the early stage. We utilize a nested flow to optimize both the extended image and velocity model.

Figure 1(a) shows a simple model with two layers and an anomaly in the upper layer. To test our approach, we start with an initial model of constant velocity, which corresponds to the upper-layer velocity, but with a 10% error. We use three extension sizes of the subsurface offset to show the behavior of our extended imaging/Born modeling. The original recorded reflection and modeled ones corresponding to a maximum $\mathbf{h} = 457$m, 305m, 152m are shown in Figure 1(b). The larger image space can reproduce the reflection with better accuracy, especially at the far offsets. We set maximum **h** to 457 m and calculate the RWI gradient for the velocity using the optimized extended image, which is shown in Figure 1(c). Figure 1(d) shows the inverted model after 10 iterations, which reveals a smooth estimation of the velocity. Both the upper layer and the anomaly are updated in the right directions.

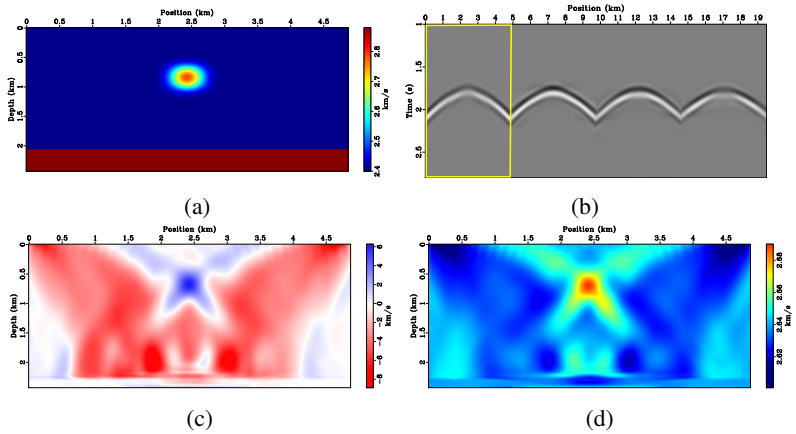

(a) (b)

(c) (d)

Figure 1 *True velocity model (a); Original recorded reflection (in yellow box) and modeled ones from extended images with maximum* $\mathbf{h}$ *equal to 457m, 305m, 152m (from left to right) (b); gradient of RWI with the extended space (c) and the inverted model after 10 iterations (d).*

Marmousi Example

Next, we apply our proposed RWI to a part of Marmousi model (Figure 2(a)). There is a water layer on top of the model to mitigate the source scattering effects. To illustrate our approach is robust against the cycle-skipping problem, we use an initial velocity linearly increasing with depth, which is shown in Figure 2(b), and apply a Butterworth filter of a 5-20Hz bandpass to the data to imitate practical conditions. There are 36 shots evenly distributed at the surface with an interval of 152m and 360 receivers at all grid points on the surface. We start with an extended image space of $\mathbf{h} = 305$m, then reduce the extension by 60m each time we converge measured based on the amount of energy in the gradient threshold.

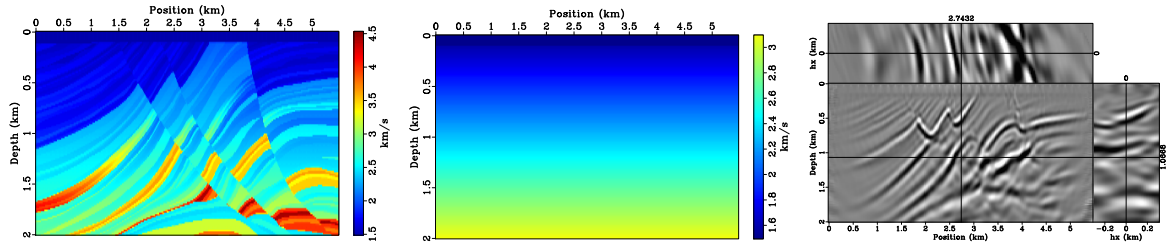

(a) (b) (c)

Figure 2 *True velocity model (a); initial model (b) and LS extended image (c) calculated from the initial model.*

The estimation of the low-wavenumber velocity components using our nested extended RWI approach is shown in Figure 3(a). Starting from the RWI model, we perform FWI and obtain the result shown in Figure 3(b). For comparison, we apply FWI starting from the velocity in Figure 2(b) and obtain a result shown in Figure 3(c). We note that our newly proposed RWI successfully retrieves the low wavenumber information, which helps FWI achieve a much better result. It is obvious that the FWI starting from the initial model, though requires more iterations with smaller steps, gets trapped into the local minima and totally fails to obtain any reasonable result. We plot vertical velocity profiles in Figures 4(a), 4(b), 4(c) and 4(d) to show the details. Our approach provides a good estimation of the model in most areas with the expected lower resolution, while FWI starting from the initial model diverges below a depth of around 400m.

Conclusions

In our RWI implementation, we still split the model into low wavenumber background and perturbations, but extend the perturbations in subsurface offset to provide the potential of fitting the data even with a poor starting model. This extension, which we gradually reduce as the velocity improves, allows us to overcome cycle skipping plaguing conventional RWI implementations. As we demonstrate with

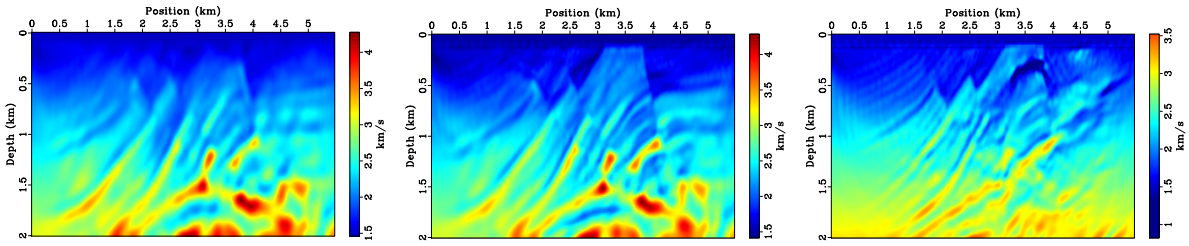

(a) (b) (c)

Figure 3 *Extended RWI result (a) and subsequent FWI (b); FWI from the linearly increasing model directly (c).*

the Marmousi example, our proposed RWI attains a reliable smooth model making a subsequent FWI converge to an accurate solution.

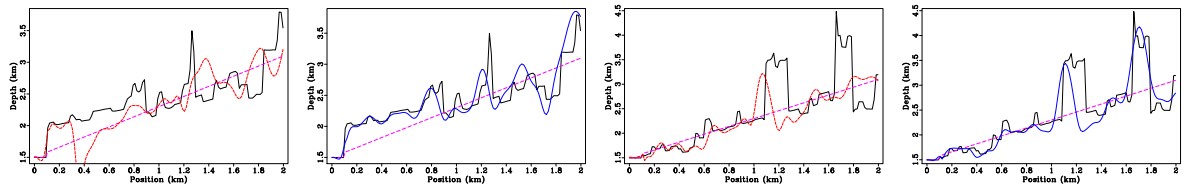

(a) (b) (c) (d)

Figure 4 *A velocity profile located at x =3.3km obtained by FWI (a) and RWI+FWI (b); A velocity profile located at x =4.0km obtained by FWI (c) and RWI+FWI (d) (black-true; pink-initial; red-FWI; blue-RWI+FWI).*

Acknowledgements

We thank KAUST for its support and the SWAG group for a collaborative environment.

References

Alkhalifah, T. and Wu, Z. [2016] The natural combination of full and image-based waveform inversion. *Geophysical Prospecting*, **64**, 19–30.

Claerbout, J.F. [1985] *Imaging the Earth's Interior*. Blackwell Scientific Publications, Inc., Cambridge, MA, USA.

Guo, Q. and Alkhalifah, T. [2016] Elastic Reflection Based Waveform Inversion in Isotropic Media. In: *78th EAGE Conference and Exhibition 2016*.

Hou, J. and Symes, W.W. [2015] An approximate inverse to the extended Born modeling operator. *GEOPHYSICS*, **80**(6), R331–R349.

Mora, P. [1989] *Inversion=migration+tomography*. Springer Berlin Heidelberg, Berlin, Heidelberg, 78–101.

Plessix, R., Roeck, Y.D. and Chavent, G. [1995] Automatic and simultaneous migration velocity analysis and waveform inversion of real data using a MBTT/WKB J formulation, 1099–1102.

Plessix, R.E. [2006] A review of the adjoint-state method for computing the gradient of a functional with geophysical applications. *Geophysical Journal International*, **167**(2), 495–503.

Symes, W.W. and Kern, M. [1994] Inversion of reflection seismograms by differential semblance analysis: algorithm structure and synthetic examples1. *Geophysical Prospecting*, **42**(6), 565–614.

Tarantola, A. [1984] Inversion of seismic reflection data in the acoustic approximation. *Geophysics*, **49**, 1259–1266.

Wu, Z. and Alkhalifah, T. [2015] Simultaneous inversion of the background velocity and the perturbation in full-waveform inversion. *Geophysics*, **80**(6), R317–R329.

Xu, S., Wang, D., Chen, F., Zhang, Y. and Lambare, G. [2012] Full Waveform Inversion for Reflected Seismic Data. *74th Conference & Exhibition incorporating SPE EUROPEC, EAGE, Extended Abstracts*.